

Spin and lattice excitations of a BiFeO₃ thin film and ceramics

S. Skiadopoulou,^{1,*} V. Goian,¹ C. Kadlec,¹ F. Kadlec,¹ X. F. Bai,² I. C. Infante,² B. Dkhil,² C. Adamo,^{3,4}
D. G. Schlom,^{3,5} and S. Kamba^{1,†}

¹*Institute of Physics, The Czech Academy of Sciences, Na Slovance 2, 182 21 Prague 8, Czech Republic*

²*Laboratoire SPMS, UMR 8580, Centrale Supélec, CNRS, Université Paris-Saclay, Grande Voie des Vignes, Chatenay-Malabry, France*

³*Department of Materials Science and Engineering, Cornell University, Ithaca, New York 14853, USA*

⁴*Department of Applied Physics, Stanford University, Stanford, California 94305, USA*

⁵*Kavli Institute at Cornell for Nanoscale Science, Ithaca, New York 14853, USA*

(Received 27 March 2015; revised manuscript received 5 May 2015; published 20 May 2015)

We present a comprehensive study of polar and magnetic excitations in BiFeO₃ ceramics and a thin film epitaxially grown on an orthorhombic (110) TbScO₃ substrate. Infrared reflectivity spectroscopy was performed at temperatures from 5 to 900 K for the ceramics and below room temperature for the thin film. All 13 polar phonons allowed by the factor-group analysis were observed in the ceramic samples. The thin-film spectra revealed 12 phonon modes only and an additional weak excitation, probably of spin origin. On heating towards the ferroelectric phase transition near 1100 K, some phonons soften, leading to an increase in the static permittivity. In the ceramics, terahertz transmission spectra show five low-energy magnetic excitations including two which were not previously known to be infrared active; at 5 K, their frequencies are 53 and 56 cm⁻¹. Heating induces softening of all magnetic modes. At a temperature of 5 K, applying an external magnetic field of up to 7 T irreversibly alters the intensities of some of these modes. The frequencies of the observed spin excitations provide support for the recently developed complex model of magnetic interactions in BiFeO₃ [R. S. Fishman, *Phys. Rev. B* **87**, 224419 (2013)]. The simultaneous infrared and Raman activity of the spin excitations is consistent with their assignment to electromagnons.

DOI: [10.1103/PhysRevB.91.174108](https://doi.org/10.1103/PhysRevB.91.174108)

PACS number(s): 78.30.-j, 63.20.-e, 75.30.Ds

I. INTRODUCTION

Among novel materials, an intense effort is concentrated on the study of multiferroics [1,2]. A wide range of applications, such as information storage, sensing, actuation, and spintronics, await pioneering materials and strategies that would produce robust magnetoelectric coupling at room temperature (RT) [3,4]. The ability to manipulate magnetization in a magnetoelectric multiferroic by electric fields can be extremely promising for such applications, due to the simplicity and cost efficiency of applying an electric field. As one of the few single-phase RT magnetoelectric multiferroics, bismuth ferrite BiFeO₃ is at the center of attention, as it presents a ferroelectric phase transition at approximately 1100 K and an antiferromagnetic one at 643 K [5].

The knowledge of lattice and spin excitations in BiFeO₃ is essential for understanding the underlying mechanisms that induce its multiferroic behavior. A series of Raman and infrared (IR) spectroscopy studies have presented controversial results concerning the assignment of the magnon and phonon modes, as well as of the highly acclaimed electromagnons (i.e., electrically active magnons). Probing IR-active low-energy excitations is hindered by a lack of sufficiently large single crystals. Raman-active phonons of the rhombohedral *R3c* BiFeO₃ structure have been reported for single crystals [6–8], polycrystalline ceramics [9–11], and thin films [12,13], however, there is a significant discrepancy between the claimed phonon frequencies and symmetry representations. A possible explanation for such inconsistencies between the various

experimental results is the presence of oblique phonon modes, which show a continuous variation of frequency along the phonon propagation vector with respect to the crystallographic axes of the probed specimen [11]. Up to now, the phonon IR spectroscopy studies have been focused on ceramics [14–16] and single crystals [17,18], whereas, to our knowledge, no report of a thin-film IR investigation exists.

When it comes to magnon and electromagnon studies, Raman spectroscopy holds the record for the number of excitations observed, yielding up to 16 magnetic modes corresponding to the cycloidal spin structure (eight Φ_n cyclon and eight Ψ_n extra-cyclon modes) for single crystals [19–22], but only one for polycrystalline thin films [23,24]. Furthermore, the influence of strain on the number of spin excitations and their frequencies were reported for epitaxial thin films grown on a series of substrates [25]. Time-domain terahertz (THz) spectroscopy [26], inelastic neutron scattering measurements [27–30], and absorbance spectroscopy in the THz range [31] have revealed modes similar to the Raman-active ones predicted by theoretical calculations [31–35]. The best agreement between the experimental and theoretical spin-excitation frequencies (including their splitting in an external magnetic field) was obtained for a microscopic model that takes into account the nearest and next-nearest neighbor exchange interactions, two Dzyaloshinskii-Moriya interactions, and an easy-axis anisotropy [31,35]. The same model successfully described the low-energy inelastic neutron scattering spectra [30]. In contrast, Komandin *et al.* [15] showed IR transmission spectra with an excitation at approximately 47 cm⁻¹ which had not been previously reported by experimental or theoretical studies. The intensive discussion in the literature concerning the nature of the spin excitations raises the question: which excitations are pure magnons (i.e., contribute only

*stella@fzu.cz

†kamba@fzu.cz

to the magnetic permeability μ) and which are electromagnons (i.e., influence at least partially the permittivity ϵ^*)? It is worth noting that according to a recent symmetry analysis [36], BiFeO₃ allows directional dichroism and therefore spin waves can be simultaneously excited by the electric and magnetic components of electromagnetic radiation. For more details on BiFeO₃ spin dynamics, see the review of Park *et al.* [37].

In the current work we report spin and lattice excitations in BiFeO₃ ceramics, as measured by the combination of IR reflectivity and time-domain THz transmission spectroscopy, in a temperature range from 10 to 900 K. All 13 IR-active phonon modes are observed, exhibiting softening on heating. Five low-frequency spin modes are detected from 5 K up to RT, the highest two appearing at 53 and 56 cm⁻¹. This corresponds to the frequency range where such excitations were theoretically predicted [31,32,35], but not experimentally confirmed up to now. At 5 K, the low-energy spin dynamics in the THz range were also studied in a varying magnetic field of up to 7 T. Softening of the (electro)magnon frequencies upon increasing the magnetic field was observed. Additionally, a BiFeO₃ epitaxial thin film grown on an orthorhombic (110) TbScO₃ single crystal substrate was studied via IR reflectance spectroscopy.

II. EXPERIMENTAL DETAILS

BiFeO₃ ceramics were prepared by the solid-state route. A stoichiometric mixture of Fe₂O₃ and Bi₂O₃ powder oxides with a purity of 99.99% was ground and uniaxially cold-pressed under 20–30 MPa pressure into 8 mm diameter pellets. The pellets were then covered by sacrificial BiFeO₃ powder to avoid bismuth oxide loss from the pellet, and sintered in a tube furnace at 825 °C for 8 h in air. To avoid any secondary phase formation, the samples were quenched to RT. Polished disks with a diameter of 4 mm and thicknesses of approximately 600 and 338 μm were used for the IR reflectivity and THz transmission measurements, respectively.

An epitaxial BiFeO₃ thin film with a thickness of 300 nm was grown by reactive molecular-beam epitaxy on a (110) single crystal substrate. The growth parameters were the same as for the samples reported in Ref. [38]. Near-normal incidence IR reflectivity spectra of the BiFeO₃ ceramics and film were obtained using a Fourier-transform IR spectrometer Bruker IFS 113v in the frequency range 20–3000 cm⁻¹ (0.6–90 THz) at RT; for the low and high temperature measurements the spectral range was reduced to 650 cm⁻¹. Pyroelectric deuterated triglycine sulfate detectors were used for the room- and high-temperature measurements up to 900 K, whereas a He-cooled (operating temperature 1.6 K) Si bolometer was used for the low-temperature measurements down to 10 K. A commercial high-temperature cell (SPECAC P/N 5850) was used for the high-temperature experiments. The thermal radiation from the hot sample entering the interferometer was taken into account in our spectra evaluation.

THz measurements from 3 to 60 cm⁻¹ (0.09–1.8 THz) were performed in the transmission mode with the use of a custom-made time-domain THz spectrometer. In this spectrometer, a femtosecond Ti:sapphire laser oscillator (Coherent, Mira) produces a train of femtosecond pulses which generates linearly polarized broadband THz pulses in a photoconducting

switch TeraSED (Giga-Optics). A gated detection scheme based on electro-optic sampling with a 1 mm thick [110] ZnTe crystal as a sensor allows us to measure the time profile of the electric field of the transmitted THz pulse. The same high-temperature cell as for the IR reflectivity was used for the THz range high-temperature measurements. Oxford Instruments Optistat optical cryostats with mylar and polyethylene windows were used for the low-temperature THz and IR measurements, respectively. THz experiments in an external magnetic field $H_{\text{ext}} \leq 7$ T were performed upon decreasing H with an Oxford Instruments Spectromag cryostat in the Voigt configuration, where the electric component of the THz radiation \mathbf{E}_{THz} was set perpendicular to H_{ext} .

The IR reflectivity and THz complex (relative) permittivity spectra $\epsilon^*(\omega)$ were carefully fit assuming the factorized form of the dielectric function based on a generalized damped-harmonic-oscillator model [39]:

$$\epsilon^*(\omega) = \epsilon_\infty \prod_{j=1}^N \frac{\omega_{\text{LO}j}^2 - \omega^2 + i\omega\gamma_{\text{LO}j}}{\omega_{\text{TO}j}^2 - \omega^2 + i\omega\gamma_{\text{TO}j}}, \quad (1)$$

where $\omega_{\text{TO}j}$ and $\omega_{\text{LO}j}$ are the frequencies of the j th transverse optical (TO) and longitudinal optical (LO) phonons, $\gamma_{\text{TO}j}$ and $\gamma_{\text{LO}j}$ are the corresponding damping constants, and ϵ_∞ denotes the high-frequency (electronic) contribution to the permittivity, determined from the RT frequency-independent reflectivity tail above the phonon frequencies. The reflectivity $R(\omega)$ is related to the complex dielectric function $\epsilon^*(\omega)$ by

$$R(\omega) = \left| \frac{\sqrt{\epsilon^*(\omega)} - 1}{\sqrt{\epsilon^*(\omega)} + 1} \right|. \quad (2)$$

To evaluate the IR reflectance spectra of the BiFeO₃/TbScO₃ thin film, a model corresponding to a two-layer optical system was used [40]. The IR reflectivity spectra of the bare TbScO₃ substrate were fit first at each temperature, using the model described by Eq. (1). The values of oscillator parameters ($\omega_{\text{TO}j}$, $\omega_{\text{LO}j}$, $\gamma_{\text{TO}j}$, $\gamma_{\text{LO}j}$, and ϵ_∞) obtained for the substrate were used for fitting the BiFeO₃/TbScO₃ thin-film spectra. The model used to describe the complex permittivity of the thin film is a sum of N independent three-parameter damped harmonic oscillators, which can be expressed as [39]

$$\epsilon^*(\omega) = \epsilon_\infty + \sum_{j=1}^N \frac{\Delta\epsilon_j \omega_{\text{TO}j}^2}{\omega_{\text{TO}j}^2 - \omega^2 + i\omega\gamma_{\text{TO}j}}, \quad (3)$$

where $\Delta\epsilon_j$ is the dielectric strength of the j th mode. Equation (3) is simpler than Eq. (1), and its use is well justified because the damping of the LO phonons of the film does not appreciably influence the reflectance spectra.

III. RESULTS AND DISCUSSION

A. Phonons in the BiFeO₃ ceramics

The temperature dependence of the experimental IR reflectivity spectra of the BiFeO₃ ceramics is shown in Fig. 1(a). The reflectivity band intensities are higher than those in the previously published spectra of ceramics [14–16] and single crystal [18], but comparable to the single-crystal spectra published by Lobo *et al.* [17]. This confirms the very high quality and density of our ceramic samples, which is

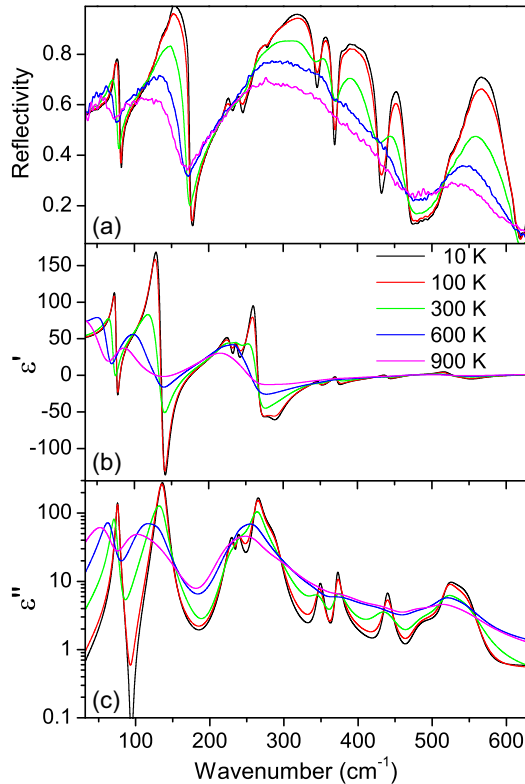


FIG. 1. (Color online) (a) IR reflectivity spectra of BiFeO₃ ceramics at selected temperatures. (b) Real and (c) imaginary part of permittivity, as obtained from the fits.

essential for an accurate determination of phonon and magnon parameters.

The IR reflectivity and THz transmission spectra were fit simultaneously using Eq. (1); the resulting phonon parameters are listed in Table I. The real and imaginary parts of the complex dielectric spectra calculated from the fits are shown in

Figs. 1(b) and 1(c). As predicted by the factor group analysis for the rhombohedral $R3c$ structure of BiFeO₃ [14], all 13 IR-active phonons ($4A_1 + 9E$ symmetries) are clearly seen from 10 K up to RT. In Table I the symmetries of all modes are assigned based on Raman spectra [11], first-principles calculations [41], and IR spectra of single crystals [17]. The damping of the modes strongly increases on heating; therefore, above 300 K, the IR reflection bands broaden and mutually overlap. Note the remarkable softening of the modes below 150 cm⁻¹ upon heating (see Fig. 1). Consequently, the static permittivity $\epsilon(0)$ determined by the sum of phonon contributions as $\epsilon(0) = \epsilon_\infty + \sum \Delta\epsilon_j$ increases on heating in agreement with the Lyddane-Sachs-Teller relation [42] (see Fig. 2). A qualitatively similar temperature dependence was published in previous studies of BiFeO₃ ceramics [14,15], but the absolute value of permittivity was lower, probably due to a lower density/quality of the earlier studied ceramics. In contrast, the permittivity calculated from the single-crystal spectra [17] is slightly higher, due to the absence of the A_1 modes whose dielectric strength $\Delta\epsilon_j$ is lower than the E -symmetry modes.

We would like to stress that the temperature dependence of permittivity calculated from the phonon contributions has been previously published mostly below RT [15,17], and only Ref. [14] reported $\epsilon(0, T)$ up to 900 K. Experimental low-frequency (i.e., below 1 MHz) dielectric data are also not available above RT due to the presence of significant leakage currents in BiFeO₃ at high temperatures. There is only one publication [16] presenting IR spectra of BiFeO₃ ceramics up to 1280 K, i.e., far above T_C , however, in this case, emissivity was measured instead of reflectivity above 600 K and $\epsilon(0, T)$ was not reported. In that work, Massa *et al.* [16] listed phonon parameters at selected temperatures, from which we recalculated $\epsilon(0, T)$; these values are presented for sake of comparison in Fig. 2. One can see that, at $T = 523$ and 850 K, Massa *et al.* [16] obtained the lowest published values of $\epsilon(0)$. We also note the unusual increase in ϵ_∞ and $\epsilon(0, T)$

TABLE I. A comparison of the parameters of the IR-active modes in the BiFeO₃ ceramics (at 10 and 900 K) and the thin film (at 10 K), obtained from IR spectra fitting. The symmetry assignment of each mode is also given.

Symmetry	Ceramics								Thin film					
	10 K				900 K				10 K ($\mathbf{E}_{\text{ext}} \parallel [1\bar{1}0]$)			10 K ($\mathbf{E}_{\text{ext}} \parallel [001]$)		
	ω_{TO}	γ_{TO}	ω_{LO}	γ_{LO}	ω_{TO}	γ_{TO}	ω_{LO}	γ_{LO}	ω_{TO}	γ_{TO}	$\Delta\epsilon$	ω_{TO}	γ_{TO}	$\Delta\epsilon$
E	75.8	4.6	81.5	2.8	64.3	40.9	70.5	19.3	74.7	1.4	4.3	77.8	1.8	4.5
E	133.7	22.8	137.4	34.6	101.0	65.1	117.9	51.1	132.2	2.3	8.6	136.7	2.9	12.2
A_1	137.8	13.6	175.8	4.0	124.3	57.6	165.8	32.9	145.2	2.4	7.4			
A_1	231.2	14.0	233.9	5.6	226.2	59.6	233.5	31.4	225.9	2.9	0.6	227.4	2.2	0.7
E	236.7	7.6	243.6	13.3	234.0	31.7	240.8	69.3	241.0	4.3	0.9	242.4	4	0.2
E	264.0	13.0	283.0	38.0	258.2	60.4	278.0	48.5	266.2	2.3	5.4	266.8	4.4	0.4
E	288.5	26.2	345.8	9.2	278.4	61.6	340.7	40.4	293.9	4.6	3.6	279.5	5.5	10.6
E	349.0	10.0	368.1	5.0	342.5	42.5	363.6	41.0						
E	372.0	7.3	430.7	10.6	364.5	50.1	420.3	51.4				371.7	9.2	0.9
E	439.6	11.0	468.0	13.3	424.0	54.3	464.3	37.1				445.7	0.3	1.1
A_1	476.2	41.2	503.7	49.1	469.8	41.0	502.8	106.2	472.2	7.1	0.01			
E	520.2	21.8	523.8	76.0	514.7	45.7	518.3	62.5	524.0	9.8	0.3	516.8	12.7	0.04
A_1	549.5	36.9	606.2	27.1	542.1	78.8	595.3	102.3	550.6	7.2	0.07	551.8	2.3	1
Spin wave												603.6	9.9	0.01

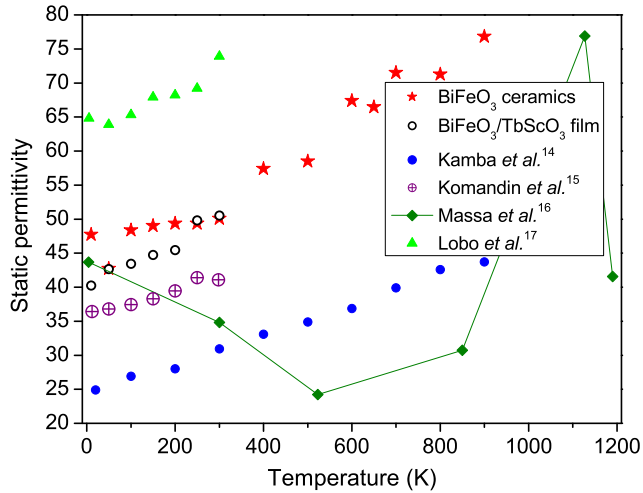


FIG. 2. (Color online) Temperature dependence of the static permittivity calculated from the sum of phonon contributions. The data for the ceramics and the film ($\mathbf{E}_{\text{ext}} \parallel [1\bar{1}0]$) from the current work are compared with previously published data obtained, on ceramics [14–16], and a single crystal [17]. The line connecting the data from Ref. [16] is a guide for the eyes. See the text for additional details.

on cooling below RT; the latter appears to be in contradiction with the soft-mode frequency increase on cooling, reported in the same work. Finally, two additional phonon modes at $T = 4$ K, not predicted by the factor-group analysis, are reported in Ref. [16]. All these facts raise questions about whether these results describe the intrinsic properties of BiFeO₃. Nevertheless, it is worth noting the peak in Massa’s data at the ferroelectric phase transition near 1120 K; this is the only experiment showing a dielectric anomaly at T_C in BiFeO₃. The peak is much lower than in other canonical ferroelectrics, apparently due to the first-order character of the phase transition from $R3c$ symmetry to the high-temperature $Pnma$ structure [5,37].

B. Excitations in the BiFeO₃ thin film

The polarized IR reflectivity spectra of the bare (110) TbScO₃ substrate and reflectance spectra of the BiFeO₃/TbScO₃ thin film are shown in Fig. 3. All BiFeO₃ mode frequencies obtained by fitting are listed in Table I. We note that, on the one hand, the BiFeO₃ phonons below 150 cm⁻¹ are better resolved in the $\mathbf{E}_{\text{ext}} \parallel [1\bar{1}0]$ polarization with respect to the substrate crystal axes, because the TbScO₃ phonons are weak in this case. On the other hand, the BiFeO₃ modes at 372 and 446 cm⁻¹ are seen only in the $\mathbf{E}_{\text{ext}} \parallel [001]$ polarized spectra, due to a more favorable TbScO₃ spectrum in this region. Namely, the large TO-LO splitting of the TbScO₃ phonons within 370–480 cm⁻¹ enhances the sensitivity of the IR reflectance to the thin-film phonons [43]. Therefore, due to the properties of TbScO₃, the two polarizations provide complementary information on the BiFeO₃ response. Note that some TbScO₃ phonons seen below 150 cm⁻¹ (see Fig. 3) exhibit anomalous temperature shifts and even splitting on cooling. This is probably caused by phonon interaction with the crystal field (and related electronic transitions) [44].

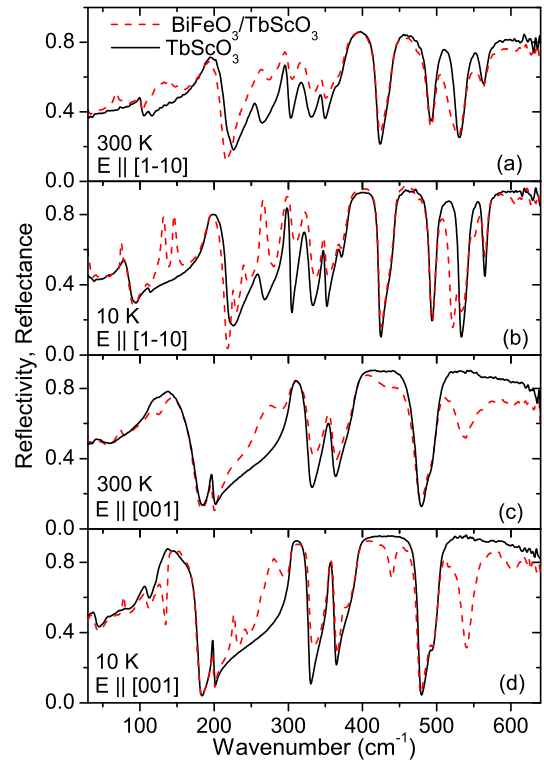


FIG. 3. (Color online) Room-temperature and 10 K IR reflectivity spectra of the TbScO₃ substrate and reflectance of the BiFeO₃/TbScO₃ thin film for polarizations (a) and (b) $\mathbf{E}_{\text{ext}} \parallel [1\bar{1}0]$ and (c) and (d) $\mathbf{E}_{\text{ext}} \parallel [001]$.

The in-plane lattice parameters of the (110) TbScO₃ substrate are slightly smaller than those of BiFeO₃, inducing only a small compressive strain ($\sim 0.24\%$) in the (001)_{cub} epitaxial film. Here the orientation of the thin film is marked with respect to the pseudocubic crystal axis (which is denoted by the subscript “cub”) of BiFeO₃. The ferroelastic and ferroelectric domain structure of BiFeO₃/TbScO₃ was investigated in Refs. [38,45], where two kinds of stripelike domains separated by (010)_{cub} vertical boundaries were reported. The spontaneous polarization \mathbf{P} in adjacent domains is rotated by 109° and its direction is tilted from the [001]_{cub} direction [45]. In our IR spectra, only vibrations polarized in the film plane are active. Since the ferroelectric polarization \mathbf{P} is tilted from the normal of the thin film plane, phonons of both E and A_1 symmetries can be excited. Nevertheless, we see only some of the modes due to our limited sensitivity to the thin film. In contrast to the ceramics samples, the phonon damping observed in the thin film is much lower (see Table I). The values of the damping constants are comparable to those of single crystals [17], which confirms the high quality of our epitaxial thin film. Similar to the case of BiFeO₃ ceramics, the phonon eigenfrequencies in the film decrease on heating, leading to an increase in the static permittivity $\epsilon(0, T)$ (see Fig. 2). The phonon frequencies of the BiFeO₃ ceramics and the film present no significant differences, which is clearly a consequence of the very small strain applied to the film by the substrate. The calculated $\epsilon(0, T)$ is, however, smaller in the BiFeO₃ film than in the single crystal (see Fig. 2), because, for

the former sample, only strong phonons were revealed in the IR reflectance spectra.

In the low-temperature $\mathbf{E}_{\text{ext}} \parallel [001]$ spectra, a weak but sharp and clearly observable minimum in reflectance develops near 600 cm^{-1} [see Fig. 3(d)]. We can exclude its phonon origin, because the factor-group analysis in rhombohedral structure does not allow an additional mode. A lower crystal symmetry is also excluded because our thin film has only 0.24% compressive strain; it is known that the films change the structure only with strain higher than 2% [46]. Also the multiphonon origin is not likely since multiphonon scattering usually decays on cooling; at RT, the peak intensity is markedly lower, close to our sensitivity limit [see Fig. 3(c)]. Interestingly, the position of the peak, approximately 604 cm^{-1} , corresponds to the maximum magnon energy observed out of the Brillouin-zone center by inelastic neutron scattering in a BiFeO₃ single crystal [27]. Therefore, we assign this peak to scattering by the highest-energy part of the magnon branch. The magnon density of states can be activated in the IR spectra due to the modulated cycloidal magnetic structure of BiFeO₃; the maxima in the density of states occur either at the maximal energy or at the Brillouin-zone boundary. Correspondingly, another peak in the density of states can be expected for the magnon branch at the K and M points. These magnons have an energy [30] of approximately 525 cm^{-1} , which falls into the range of the highest-energy phonon. We assume that this strong phonon screens the weak magnon signal, which is why we do not detect the corresponding absorption in the IR spectra. Finally, let us mention that the magnons from the Brillouin-zone boundary become frequently electrically active due to the exchange striction [47]; therefore, they can be called electromagnons.

C. Magnetic excitations in THz spectra of BiFeO₃ ceramics

Our efforts to measure THz spectra of the BiFeO₃ film failed, due to insufficient signal. This can be explained by the fact that the thin film only slightly absorbs the THz waves and the index of refraction n of BiFeO₃ is higher than that of the substrate only by $\approx 50\%$. We note that time-domain THz spectroscopy can be used only for studies of the thin films with n at least one order of magnitude higher than that of the substrate. As an example, such a technique was successfully used for investigation of the ferroelectric soft mode behavior near a strain-induced ferroelectric phase transition in SrTiO₃ thin films [48].

In contrast, THz spectra of the BiFeO₃ ceramics were successfully measured at temperatures from 5 to 900 K. The spectra of the complex refractive index $N(\omega) = n(\omega) + ik(\omega)$, determined from experimental data for various temperatures, are presented in Fig. 4. In magnetic systems, N depends on the complex permittivity ε^* and permeability μ^* via the relationship $N(\omega) = \sqrt{\mu^* \varepsilon^*}$. Since we cannot resolve whether the observed modes contribute to μ^* (as magnons) or ε^* (as electromagnons or polar phonons), we only present $n(\omega)$, $k(\omega)$ spectra in Fig. 4.

In the THz spectra, one can see a gradual increase in n and k on heating. This is mainly caused by the softening of the TO₁ phonon and an increase in the phonon damping with heating. The weak maxima in the $k(\omega)$ spectra correspond

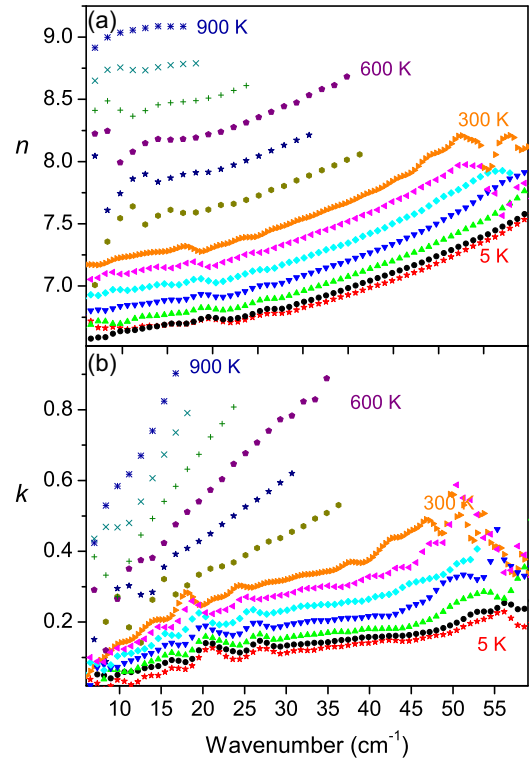


FIG. 4. (Color online) Temperature dependencies of the (a) refractive index and (b) extinction coefficient spectra of BiFeO₃ ceramics, determined from the THz transmission. The spectra are shown for every 50 and 100 K below and above RT, respectively.

to frequencies of magnetic excitations. Their temperature dependences are plotted in Fig. 5 together with the modes observed in Raman [20,21] and IR [26,31] spectra. Note that the modes between 32 and 44 cm^{-1} become IR active only in external magnetic field [31,35]. Besides a good agreement between the frequencies of Raman and IR-active modes, one can see a gradual decrease in all mode frequencies with increasing temperature. Although the excitations should exist at least up to T_N , we fit our THz spectra only up to 300 K, because, above RT, their damping is very high, precluding their exact fitting. We clearly distinguish five magnetic excitations. The three of them appearing up to 27 cm^{-1} correspond to the IR-active modes observed earlier by other authors [15,26,31]. In our spectra they exhibit an enhanced damping in comparison with single-crystal data, mainly due to the fact that we measured unpolarized spectra. At 5 K, two modes are seen with peak absorption frequencies of 53 and 56 cm^{-1} . These modes were not observed in IR spectra before, apparently because the samples used in previous studies were opaque above 40 cm^{-1} . These peak frequencies correspond well to the Ψ_7 and Φ_8 modes reported in Raman spectra by Cazayous *et al.* [20]. Note that Komandin *et al.* [15] predicted a polar and heavily damped mode at an estimated frequency of 47 cm^{-1} , but their rough estimation was based on discrepancies between IR reflectivity and THz transmission spectra. Nagel *et al.* [31] discovered additional spin excitations near 40 and 43 cm^{-1} , but a magnetic field higher than 5 T was needed for the activation of these excitations in far-IR transmission spectra. Furthermore, Fishman predicted [35] a mode above 50 cm^{-1} ,

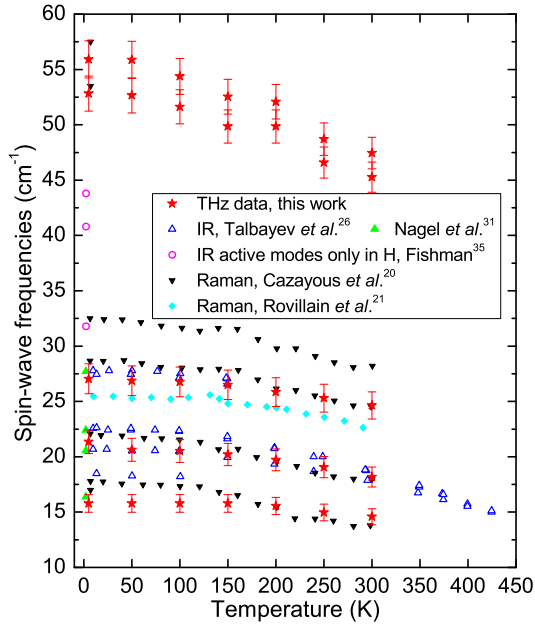


FIG. 5. (Color online) Temperature dependence of the spin-excitation frequencies determined by fits of the absorption index spectra in the THz range compared with published frequencies obtained from Raman scattering [20,21] and far IR spectra [31]. The modes at ~ 32 , 41, and 44 cm^{-1} were predicted by Fishman [35] and they become IR active only in magnetic field above 7 T [31].

which should soften in an external magnetic field, and de Sousa *et al.* predicted [32] exactly the two modes which we observe.

We measured THz transmittance at 5 K under a magnetic field up to 7 T [see the $k(\omega)$ spectra in Fig. 6]. All modes exhibit small frequency shifts with increasing magnetic field. A similar behavior was reported by Nagel *et al.* [31], but their frequency shifts were higher due to much higher values of the applied magnetic field (up to 31 T). We see also weak indications of the modes near 32, 35, 38, and 42 cm^{-1} , which correspond well (except the one at 35 cm^{-1}) to the magnetic-field induced

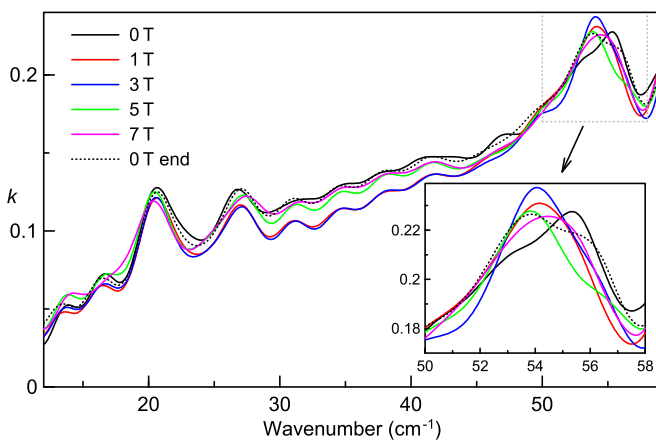


FIG. 6. (Color online) Magnetic field dependence of the experimental THz extinction coefficient in the BiFeO_3 ceramics measured at 5 K. The dotted line shows the zero-field spectrum after applying the magnetic field.

modes of Ref. [31]. In our measurements, while the sample was kept at a temperature of 5 K, applying the magnetic field of 7 T irreversibly changed the shape of the magnetic modes in the absorption index spectrum (see Fig. 6), similarly to the observations in Ref. [31]. This behavior is probably a consequence of magnetic-field-induced changes in the geometry of magnetic domains and pinning the domain walls on defects. The pronounced modes near 53 and 56 cm^{-1} can be identified with the pair of modes predicted by Fishman near 45 cm^{-1} at $H_{\text{ext}} = 15$ T [35]. Thus, our observations confirm the complex effective Hamiltonian describing the magnetic interactions in BiFeO_3 ; it includes nearest and next-nearest neighbor exchange interactions, two Dzyaloshinskii-Moriya interactions, and an easy-axis anisotropy [35]. Very recently this model was also confirmed by low-energy inelastic neutron scattering spectra [30].

We were not able to fit unambiguously the THz spectra above 300 K using the modes seen at low temperatures, owing to their heavy damping at high temperatures. Nevertheless, a fit with one effective overdamped mode provided reasonable results. Surprisingly, this overdamped mode with a relaxation frequency around 15 cm^{-1} and $\Delta\varepsilon = 0.5\text{--}1.2$ ($\Delta\varepsilon$ rising with T) was necessary even above T_N , suggesting that there are still some paramagnons present in the paramagnetic phase. Alternatively, this mode might be due to a multiphonon or quasi-Debye absorption allowed in the noncentrosymmetric phase [49].

Finally, we would like to stress that from unpolarized THz spectra, we could not distinguish whether our magnetic excitations are magnons or electromagnons. The symmetry analysis published by Szaller *et al.* [36], however, allows electromagnons in the cycloidal G -type antiferromagnetic phase of BiFeO_3 . In analogy with selection rules for polar phonons which, in acentric lattices, are both IR and Raman active, we suggest that for spin excitations, their simultaneous IR and Raman activities indicate that they are electromagnons. During the review process of this paper, the polar activity of spin excitations has been confirmed by Kézsmárki *et al.* [50], who observed directional dichroism [36,51] of a BiFeO_3 single crystal in polarized far-IR spectra between 10 and 30 cm^{-1} .

IV. CONCLUSIONS

An extensive study of IR vibrational spectra of BiFeO_3 ceramics and an epitaxial thin film is reported. The intensities of all phonons observed in the ceramics are higher than in the previous publications [14–16]. Thus, the static permittivity of our samples calculated from phonon contributions is close to the previously published single crystal data [17]. Some phonons slightly soften on heating, leading to an increase in the permittivity towards T_C . Nevertheless, the permittivity is much lower than in canonical ferroelectric perovskites, such as BaTiO_3 and KNbO_3 , because the phonons in BiFeO_3 are much harder and the Born effective charges are much smaller. In addition, the phonons in a $\text{BiFeO}_3/\text{TbScO}_3$ epitaxial thin film were studied, showing parameters similar to those in BiFeO_3 single crystals. In the thin film, an additional weak excitation

near 600 cm⁻¹ was detected, which apparently corresponds to a peak in the magnon density of states possibly activated due to the incommensurately modulated magnetic structure of BiFeO₃. Time-domain THz spectra of BiFeO₃ ceramics reveal most of the spin excitations previously observed in single crystals [26,31]. Also, at 5 K, a pair of IR-active modes near 55 cm⁻¹ were observed, which corresponds to spin excitations theoretically predicted by de Sousa *et al.* [32] and Fishman [35]. This observation confirms the particular form of the Hamiltonian suggested by Fishman for the explanation of the magnetic interactions in BiFeO₃.

ACKNOWLEDGMENTS

This work was supported by the Czech Science Foundation (Projects P204/12/1163 and 15-08389S), MŠMT Project LH13048, and by European Union funding under the 7th Framework Programme (Project NOTEDEV). The work at Cornell was supported by the National Science Foundation through the Penn State Center for Nanoscale Science, DMR-1420620. The work at Chatenay Malabry has been supported by the French ANR program NOMILOPS (ANR-11-BS10-016-02) project. X. F. Bai also wishes to thank the China Scholarship Council (CSC) for funding his stay in France.

-
- [1] M. Fiebig, *J. Phys. D: Appl. Phys.* **38**, R123 (2005).
- [2] Y. Tokura, S. Seki, and N. Nagaosa, *Rep. Prog. Phys.* **77**, 076501 (2014).
- [3] W. Eerenstein, N. D. Mathur, and J. F. Scott, *Nature (London)* **442**, 759 (2006).
- [4] N. A. Spaldin, S. W. Cheong, and R. Ramesh, *Phys. Today* **63**, 38 (2010).
- [5] G. Catalan and J. F. Scott, *Adv. Mater.* **21**, 2463 (2009).
- [6] R. Haumont, J. Kreisel, P. Bouvier, and F. Hippert, *Phys. Rev. B* **73**, 132101 (2006).
- [7] H. Fukumura, S. Matsui, H. Harima, T. Takahashi, T. Itoh, K. Kisoda, M. Tamada, Y. Noguchi, and M. Miyayama, *J. Phys.: Condens. Matter* **19**, 365224 (2007).
- [8] R. Palai, H. Schmid, J. F. Scott, and R. S. Katiyar, *Phys. Rev. B* **81**, 064110 (2010).
- [9] D. Kothari, V. R. Reddy, V. G. Sathe, A. Gupta, A. Banerjee, and A. M. Awasthi, *J. Magn. Magn. Mater.* **320**, 548 (2008).
- [10] D. Rout, K.-S. Moon, and S.-J. L. Kang, *J. Raman Spectrosc.* **40**, 618 (2009).
- [11] J. Hlinka, J. Pokorný, S. Karimi, and I. M. Reaney, *Phys. Rev. B* **83**, 020101 (2011).
- [12] M. K. Singh, H. M. Jang, S. Ryu, and M.-H. Jo, *Appl. Phys. Lett.* **88**, 042907 (2006).
- [13] R. Palai, J. F. Scott, and R. S. Katiyar, *Phys. Rev. B* **81**, 024115 (2010).
- [14] S. Kamba, D. Nuzhnyy, M. Savinov, J. Šebek, J. Petzelt, J. Prokleška, R. Haumont, and J. Kreisel, *Phys. Rev. B* **75**, 024403 (2007).
- [15] G. A. Komandin, V. I. Torgashev, A. A. Volkov, O. E. Porodinkov, I. E. Spektor, and A. A. Bush, *Phys. Solid State* **52**, 734 (2010).
- [16] N. E. Massa, L. del Campo, D. de Souza Meneses, P. Echegut, G. F. L. Fabbris, G. d. M. Azevedo, M. J. Martinez Lope, and J. A. Alonso, *J. Appl. Phys.* **108**, 084114 (2010).
- [17] R. P. S. M. Lobo, R. L. Moreira, D. Lebeugle, and D. Colson, *Phys. Rev. B* **76**, 172105 (2007).
- [18] J. Lu, M. Schmidt, P. Lunkenheimer, A. Pimenov, A. A. Mukhin, V. D. Travkin, and A. Loidl, *J. Phys.: Conf. Series* **200**, 012106 (2010).
- [19] M. K. Singh, R. S. Katiyar, and J. F. Scott, *J. Phys.: Condens. Matter* **20**, 252203 (2008).
- [20] M. Cazayous, Y. Gallais, A. Sacuto, R. de Sousa, D. Lebeugle, and D. Colson, *Phys. Rev. Lett.* **101**, 037601 (2008).
- [21] P. Rovillain, M. Cazayous, Y. Gallais, A. Sacuto, R. P. S. M. Lobo, D. Lebeugle, and D. Colson, *Phys. Rev. B* **79**, 180411 (2009).
- [22] P. Rovillain, R. de Sousa, Y. Gallais, A. Sacuto, M. A. Méasson, D. Colson, A. Forget, M. Bibes, A. Barthélémy, and M. Cazayous, *Nat. Mater.* **9**, 975 (2010).
- [23] A. Kumar, J. F. Scott, and R. S. Katiyar, *Appl. Phys. Lett.* **99**, 062504 (2011).
- [24] A. Kumar, J. F. Scott, and R. S. Katiyar, *Phys. Rev. B* **85**, 224410 (2012).
- [25] D. Sando, A. Agbelele, D. Rahmedov, J. Liu, P. Rovillain, C. Toulouse, I. C. Infante, A. P. Pyatakov, S. Fusil, E. Jacquet *et al.*, *Nat. Mater.* **12**, 641 (2013).
- [26] D. Talbayev, S. A. Trugman, S. Lee, H. T. Yi, S.-W. Cheong, and A. J. Taylor, *Phys. Rev. B* **83**, 094403 (2011).
- [27] J. Jeong, E. A. Goremychkin, T. Guidi, K. Nakajima, G. S. Jeon, S.-A. Kim, S. Furukawa, Y. B. Kim, S. Lee, V. Kiryukhin *et al.*, *Phys. Rev. Lett.* **108**, 077202 (2012).
- [28] O. Delaire, M. B. Stone, J. Ma, A. Huq, D. Gout, C. Brown, K. F. Wang, and Z. F. Ren, *Phys. Rev. B* **85**, 064405 (2012).
- [29] Z. Xu, J. Wen, T. Berlijn, P. M. Gehring, C. Stock, M. B. Stone, W. Ku, G. Gu, S. M. Shapiro, R. J. Birgeneau *et al.*, *Phys. Rev. B* **86**, 174419 (2012).
- [30] J. Jeong, M. D. Le, P. Bourges, S. Petit, S. Furukawa, S.-A. Kim, S. Lee, S.-W. Cheong, and J.-G. Park, *Phys. Rev. Lett.* **113**, 107202 (2014).
- [31] U. Nagel, R. S. Fishman, T. Katuwal, H. Engelkamp, D. Talbayev, H. T. Yi, S.-W. Cheong, and T. Rößm, *Phys. Rev. Lett.* **110**, 257201 (2013).
- [32] R. de Sousa and J. E. Moore, *Phys. Rev. B* **77**, 012406 (2008).
- [33] R. S. Fishman, N. Furukawa, J. T. Haraldsen, M. Matsuda, and S. Miyahara, *Phys. Rev. B* **86**, 220402 (2012).
- [34] R. S. Fishman, J. T. Haraldsen, N. Furukawa, and S. Miyahara, *Phys. Rev. B* **87**, 134416 (2013).
- [35] R. S. Fishman, *Phys. Rev. B* **87**, 224419 (2013).
- [36] D. Szaller, S. Bordács, V. Kocsis, T. Rößm, U. Nagel, and I. Kézsmárki, *Phys. Rev. B* **89**, 184419 (2014).
- [37] J.-G. Park, M. D. Le, J. Jeong, and S. Lee, *J. Phys.: Condens. Matter* **26**, 433202 (2014).

- [38] C. T. Nelson, P. Gao, J. R. Jokisaari, C. Heikes, C. Adamo, A. Melville, S.-H. Baek, C. M. Folkman, B. Winchester, Y. Gu *et al.*, *Science* **334**, 968 (2011).
- [39] F. Gervais, *Infrared and Millimeter Waves* (Academic, New York, 1983), Vol. 8, Chap. 7, p. 279.
- [40] V. Železný, I. Fedorov, and J. Petzelt, *Czech. J. Phys.* **48**, 537 (1998).
- [41] P. Hermet, M. Goffinet, J. Kreisel, and P. Ghosez, *Phys. Rev. B* **75**, 220102 (2007).
- [42] R. H. Lyddane, R. G. Sachs, and E. Teller, *Phys. Rev.* **59**, 673 (1941).
- [43] V. Goian, S. Kamba, N. Orloff, T. Birol, C. H. Lee, D. Nuzhnyy, J. C. Booth, M. Bernhagen, R. Uecker, and D. G. Schlom, *Phys. Rev. B* **90**, 174105 (2014).
- [44] S. Kamba, V. Goian, D. Nuzhnyy, V. Bovtun, M. Kempa, J. Prokleška, M. Bernhagen, R. Uecker, and D. G. Schlom, *Phase Transitions* **86**, 206 (2013).
- [45] C. M. Folkman, H. W. Jang, C. B. Eom, C. T. Nelson, X. Q. Pan, Y. L. Li, L. Q. Chen, A. Kumar, V. Gopalan, and S. K. Streiffer, *Appl. Phys. Lett.* **94**, 251911 (2009).
- [46] D. Sando, A. Barthélémy, and M. Bibes, *J. Phys.: Condens. Matter* **26**, 473201 (2014).
- [47] M. P. V. Stenberg and R. de Sousa, *Phys. Rev. B* **85**, 104412 (2012); **80**, 094419 (2009).
- [48] D. Nuzhnyy, J. Petzelt, S. Kamba, P. Kužel, C. Kadlec, V. Bovtun, M. Kempa, J. Schubert, C. M. Brooks, and D. G. Schlom, *Appl. Phys. Lett.* **95**, 232902 (2009).
- [49] A. Tagantsev, V. Sherman, K. Astafiev, J. Venkatesh, and N. Setter, *J. Electroceram.* **11**, 5 (2003).
- [50] I. Kézsmárki, U. Nagel, S. Bordács, R. S. Fishman, J. H. Lee, H. T. Yi, S.-W. Cheong, and T. Rőöm, [arXiv:1505.00033](https://arxiv.org/abs/1505.00033).
- [51] Y. Takahashi, R. Shimano, H. Murakawa, and Y. Tokura, *Nat. Phys.* **8**, 121 (2012).